IEEE Access
Multidisciplinary | Rapid Review | Open Access Journal

Received 9 March 2023, accepted 19 March 2023, date of publication 22 March 2023, date of current version 29 March 2023.

Digital Object Identifier 10.1109/ACCESS.2023.3260219

RESEARCH ARTICLE

Digital Interactive Design and Robot-Assisted Preparation Experiment of Tooth Veneer Preparation: An in Vitro Proof-of-Concept

SUN JIAN-PENG[1], JIANG JIN-GANG[1,2], (Member, IEEE), QIAN WEI[1], HUANG ZHI-YUAN[3], MA HONG-YUAN[1,4], AND ZHOU SHAN[5]

[1]Key Laboratory of Advanced Manufacturing and Intelligent Technology, Ministry of Education, Harbin University of Science and Technology, Harbin, Heilongjiang 150080, China
[2]Robotics and its Engineering Research Center, Harbin University of Science and Technology, Harbin 150080, China
[3]State Key Laboratory of Robotics and System, Harbin Institute of Technology, Harbin, Heilongjiang 150001, China
[4]Harbin Branch of Taili Communication Technology Ltd., China Electronics Technology Group Corporation, Harbin, Heilongjiang 150080, China
[5]Second Affiliated Hospital of Harbin Medical University, Harbin, Heilongjiang 150081, China

Corresponding author: Jiang Jin-Gang (jiangjingang@hrbust.edu.cn)

This work was supported in part by the Natural Science Foundation of Heilongjiang Province under Grant LH2021E081, in part by the Fundamental Research Foundation for Universities of Heilongjiang Province under Grant LGYC2018JQ016, and in part by the Research Launch Foundation for Heilongjiang Province Postdoctoral.

ABSTRACT In the fixed prosthesis process dental prosthesis treatment, the dentist needs to conceive the morphology of the tooth preparation and make numerous micro-adjustments by manual operation. This study aims to establish a digital design system for accurate designing of veneer preparation and study the trajectory planning of the robot-assisted preparation. According to the standard operation requirements, the projection line segmentation method based on point drawing is proposed for interactive selection to ensure the margin smoothness of the preparation area. The preparation depth is parameterized, and the foldback point correction method based on secondary segmentation is used for repairing the offset preparation area to ensure surface smoothness. The fenestration preparation model was obtained in the digital interactive design software. The model is divided into two feature areas which are interpolated by the B-spline curve and NURBS surface, respectively. The isoparametric curve method is used to plan the preparation trajectory. The experimental and theoretical values of the target feature points from the X, Y and Z coordinate directions were also calculated and analyzed. The experiment is carried out by the physical prototype of the tooth preparation robot. The maximum error of the feature points on the preparation are 0.180 mm, 0.104 mm and 0.142 mm in X, Y and Z directions, respectively. The confidence interval of the system error is stable within 0.30 mm. The error of the feature points verifies the feasibility of the digital interactive design system and the correctness of the trajectory planning of tooth veneer preparation. The system could have the potential to assist dentists in the precise design of the veneer preparation, improve the processing efficiency and ensure the effect of tooth veneer prosthesis.

INDEX TERMS Dental robot, tooth preparation, interactive design, robot trajectory planning, mesh segmentation.

I. INTRODUCTION

Dental defects seriously affect the oral health and facial aesthetics of patients. Modern prosthetics not only require functional recovery but also gradually integrate into oral aesthetics to achieve the transformation from functional recovery to functional and aesthetic dual needs [1], [2], [3], especially for anterior teeth veneer prosthetics. The veneer aesthetic prosthesis is a minimally invasive restorative technique that takes into account both aesthetics and biology for anterior teeth with caries, discoloration, large gaps, malocclusion, partial loss, and mild torsion [4], [5].

The associate editor coordinating the review of this manuscript and approving it for publication was Gyorgy Eigner.

Tooth preparation is a necessary part of the treatment for veneer prosthesis, which is an operation in which the dentist quantitatively removes the hard tissue from the affected tooth and forms the desired three-dimensional morphology, providing installation space, bonding surface, and margin line for the porcelain veneer prosthesis [6]. Tooth preparation for complete coronal restoration usually adopts standardized parameters, which can reach 2 mm and have a certain fault tolerance [7]. Unlike complete coronal restoration, veneer preparation preserves the original tooth body as much as possible, the preparation morphology is more personalized, and the requirements for preparation parameters are stricter than coronal restoration. Excessive preparation may cause dentin exposure, decreased marginal closure, poor bonding, and even pulp congestion and inflammation. Poor preparation leads to inadequate marginal fit or deficient crown contour and cannot improve tooth color [8], [9]. Traditional veneer preparation depends on the rich clinical experience of dentists, who need to preconceive the morphology of the preparation based on different patients' dental conditions before operation. It is impossible to quantify and visualize the morphology of the target tooth, so it is not easy to accurately design the preparation. A large number of repetitive micro-adjustments of the target tooth need to be performed in combination with manual operations, and it is difficult to avoid visual deviations of the human eyes and manual positioning control errors, making it difficult for the precision of the preparation to meet individualized expected restorative results and manual operation is inefficient [7]. Therefore, there is an urgent need to adopt digital and automated technologies in oral prosthetics to ensure the precise design and processing quality of tooth preparations.

Accurate morphological design is the primary task of automated preparation [10]. In recent years, digital technologies such as optical scanning, CAD/CAM and 3D printing [11], [12] have been gradually applied in the field of restorative dentistry. With the development of digital dentistry, various assisted prosthodontic systems have emerged in turn. Gontijo et al. [13] proposed DSD (Digital smile design), which outlines the aesthetic information of the patient's teeth and face to help the surgeon analyze and design the treatment plan. It can show patients the effect of veneer restoration, but does not provide robotic trajectory planning for robot-assisted tooth preparation. Reference [14] designed an SLA dental preparation guide with multiple guide holes to effectively control the preparation depth of the tooth axial surface and margins. Although this method can control the preparation depth, the accuracy of the preparation still needs to be perfected to simply prevent over-preparation. Silva et al. [15] generated a sequence of 3D printed guides using the First Fit system for the preparation of veneers for specialized dental handpieces. However, a precise preparation design has not been achieved and the actual operation still needs to be performed manually. Therefore, in preparation design, [10] designed marginal, occlusal, and axial preparation areas for complete crown restorations of first molars based on Geomagic and Imageware software to assist in trajectory planning of dental preparations [7] used a semi-automatic interactive approach to design marginal lines for dental preparations to achieve feature parameter-based modeling of complete crown preparations. This system quickly and accurately enabled individualized design of parameters such as shoulder width and convergence angle. In summary, the existing digital methods can be well used for modeling of standardized full crown preparations and for the design and fabrication of various restorations. However, there are many types of veneer preparation, which are highly individualized and require high smoothness and flatness. It is difficult to reflect the ideal morphology of the preparation by standardized parameters alone. Currently, no digital design methods and systems dedicated to veneer preparation have been developed. In dental automation, robot-assisted dentists can effectively improve the accuracy and reduce the risk of dental processing [16], [17]. Kan et al. [18] designed a human-robot collaborative implant system (HRCDIS), which is based on a zero-force hand-guided concept and an operational task management workflow that enables highly accurate and stable osteotomy drilling during implant surgery based on the surgeon's decision and the robot arm's movement. Li et al. [19] used a tendon sheath mechanism combined with a pneumatically actuated silicone soft support actuator to improve the stiffness and flexibility of the system in a dental manipulator that can be widely used for caries removal and tooth preparation. Otani et al. [20] designed a tooth preparation robot with a motorized high-speed dental handpiece mounted on the end of the manipulator, which was then used with a 3D laser scanner to scanning the tooth model. The robot prepared the teeth according to the designed preparation model, which is similar to the idea of this study. Yuan et al. [21], [22] developed a 6-DOF dental preparation robotic system based on a laser 3D engraver. The laser beam is introduced into the laser working head through the guide arm and is fixed to the oral cavity through the tooth positioner. The laser working head controls the movement of the laser to complete the tooth preparation. Our team cite24, 25 proposed an augmented reality-based robot to assist in the complete crown preparation of posterior teeth. NURBS curves and NURBS surfaces were used for inverse calculation and interpolation to achieve trajectory planning for robot-assisted preparation. In summary, robotic applications for assisted full crown preparation have emerged, while trajectory planning methods suitable for veneer preparation have not been investigated.

The main focus of this work is to propose a digital interactive design method for tooth veneer preparation. A projection line segmentation method based on point drawing was proposed to ensure the margin smoothness of the personalized preparation area. In order to ensure the surface flatness of the preparation, the preparation depth is parameterized, and a foldback point correction method based on secondary segmentation is proposed to repair the preparation area after the offset. To adapt the

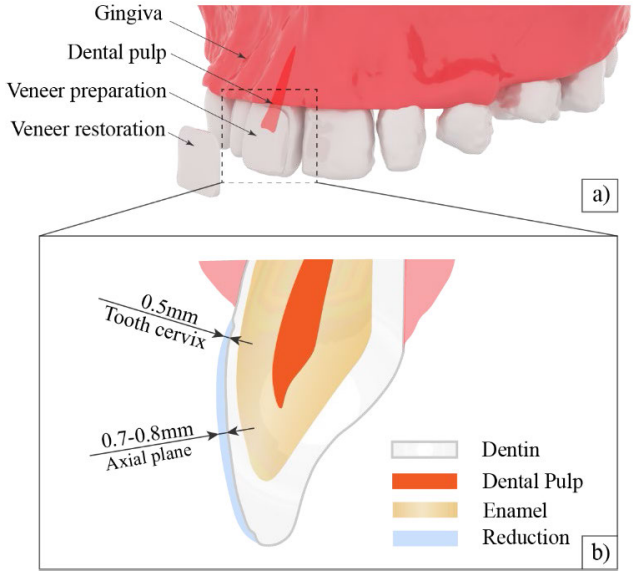

FIGURE 1. The fenestration preparation morphology. a) Morphology of veneer preparation and restoration. b) Preparation parameters.

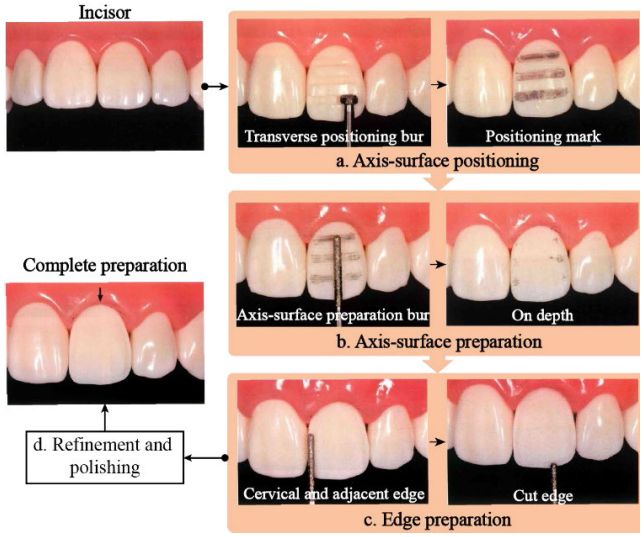

FIGURE 2. Flow chart of fenestration preparation.

different morphological features, the preparation model was divided into finishing lines preparation area and axial surface preparation area. Then the two areas were interpolated based on the B-spline curve and NURBS surface to complete the trajectory planning respectively. Finally, the prototype of the veneer preparation robot was built and relevant experiments were carried out.

II. VENEER PREPARATION PROCESS ANALYSIS

A. VENEER PREPARATION REQUIREMENTS AND PROCESS

Veneer restoration requires relatively minimal preparation depth, with the preparation generally occurring in the enamel layer. Dentists expect sub-millimeter precision in tooth preparations. The depth of tooth preparation for the adjacent surface, tooth neck, and axial surface is 0.5∼1 mm, 0.3∼0.5 mm, and 0.7∼0.8 mm, respectively. Moreover, the preparation depth for the cutting end can reach 1.5 mm. The fenestration preparation is the preferred conservative treatment method with a minor depth of dental tissue abrasion. Its preparation parameters are shown in Fig. 1. The fenestration preparation can be seated directly from the axial surface without modifying the crown length, with high loading capacity and marginal adaptation. Therefore, the fenestration preparation was selected as the main target of this study.

B. VENEER PREPARATION INTERACTIVE DESIGN SCHEME

It can be seen from Fig. 2 that the preparation includes axial surface area and margin area. Considering the clinical requirements, for the design of the axial surface area mainly to ensure its flatness, make it as close as possible to the natural axial surface morphology, ensure the tightness between it and the restoration; While the margin area should create a good retention space for the veneer restoration, form a margin platform with a suitable width, and ensure the smoothness of the curve. There should be no sharp corners and edge fins to ensure margin tightness and avoid stress concentration. Due to the conservative principle of veneer preparation, namely preserve the healthy tissue as much as possible, which leads to the personalized margin characteristics of the preparation, the curve shape cannot be accurately quantified only through parameter adjustment, so it needs to be determined by interactive drawing. In addition, the preparation depth should be parameterized, and a layer-by-layer design is also required for robot processing. The digital interactive design scheme for preparations is shown in Fig. 3.

C. DEVELOPMENT OF INTERACTIVE DESIGN SOFTWARE FOR VENEER PREPARATION

1) MODEL PREPROCESSING AND TOPOLOGY RECONSTRUCTION

Considering the requirements for the surface accuracy of the tooth preparation, the tooth surface data were obtained by the oral scanning with precision of 0.02mm. However, the storage form of directly obtained data in STL format is redundant, the efficiency of accessing and maintaining arrays is low, the vertices of the triangle array are repeatedly stored many times. Therefore, it is solved from two aspects: (a) Mesh simplification; (b) Reconstruction of the topological sequence of the mesh model and adopting a more efficient storage form [26].

On the premise of maintaining the tooth model morphology, the edge collapse method based on the minimum quadratic error measurement is used in this study, which is fast in calculation and relatively complete in retaining the geometric information. It can process the human bone mesh model [27]. Our simplified principle and results are shown in Fig. 4. The number of patches before simplification is 435254, and after simplification is 3355.

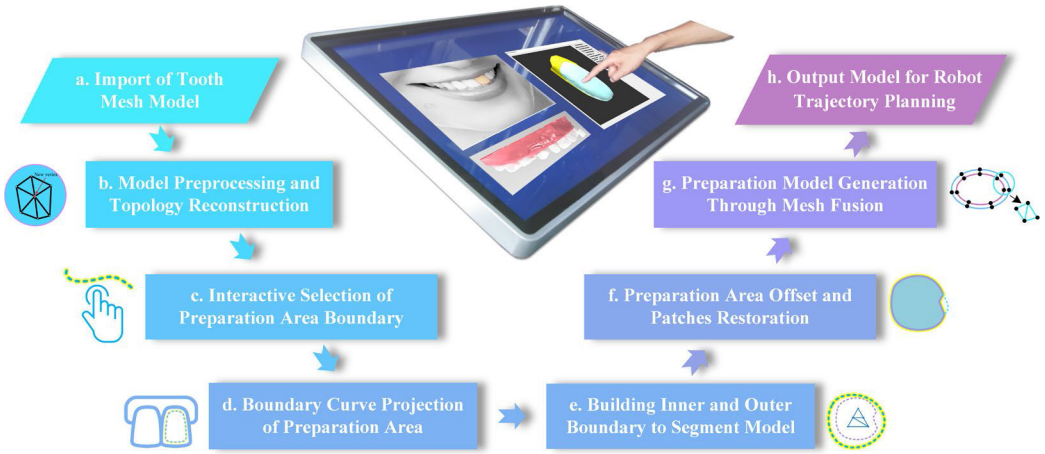

FIGURE 3. Digital interactive design scheme for preparations.

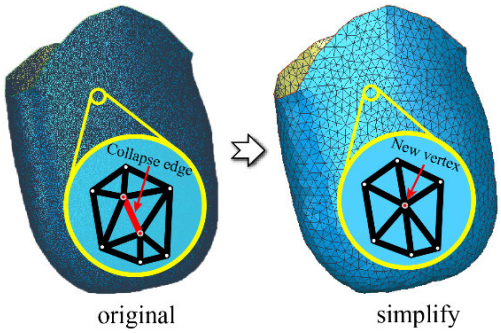

FIGURE 4. Results of mesh model simplification.

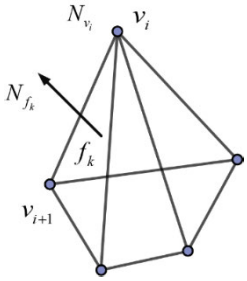

FIGURE 5. The relationship between vertex and neighborhood patches.

By constructing the vertex array of the mesh model, the edges of the triangle patch can be accessed by using the vertex indices of the first and last points in the maintained vertex array; the triangle vertices are arranged in a counterclockwise order, where the vertex index and the normal vector of the triangle patch need to be stored. The improved storage format is as follows: The correspondence between each vertex and its neighborhood is established, as shown in Fig. 5. All triangle patches are traversed and the occurrence number of each vertex index is recorded, namely, the number of one neighborhood vertex and one neighborhood patch of each vertex v_i. The patch array index is maintained, all the patch indices containing vertex v_i are recorded and stored in one neighborhood patch. Access a neighborhood patch of v_i, and the index of the dissimilar point v_{i+1} of v_i in the patch is recorded as a neighborhood vertex (v_i). The topological sequence of the mesh is established and any vertex can be accessed, and the patch and vertex information of a neighborhood can be obtained, thereby improving the access efficiency. This storage form filters out redundant model vertices, and the efficiency of accessing and maintaining arrays is significantly improved.

2) INTERACTIVE SELECTION OF PREPARATION AREA BOUNDARY

During the fenestration preparation, the formation of the preparation area mainly depends on the acquisition of the margin curve, and the margin smoothness determines the stability and tightness of the retention between veneer preparation and restoration. In the digital design for restorations, the automatic identification and extraction of feature lines at the junction of teeth and gums are often used as the reference [28]. This method has a good effect on the preparation of posterior crowns, but it is not suitable for the veneer preparation where the preparation area is distributed on the labial side. Considering the personalized needs and conservative principles of the preparation, an interactive design method was adopted by this paper, which allows doctors to select the preparation area interactively with preoperative images and professional knowledge.

In order to facilitate the adjustment of the drawing area, this paper selects the point drawing method to form the curve without setting parameters. Doctors select control points on the screen and introduce B-spline curves to fit the boundary points, which can realize dragging/increasing control points to fine-tune local shapes. However, the coordinates selected on the screen are 2D pixel coordinates. In order to fit the spatial curve, it is necessary to transform the pixel coordinates into 3D space coordinates. Referring to the camera imaging principle in image processing, first, the photographed object is transformed from the world coordinate system to the camera coordinate system. The transformation matrix of the

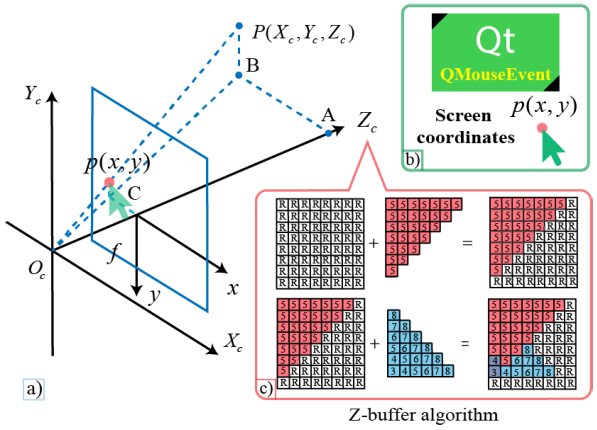

FIGURE 6. a) Camera perspective projection principle. b) Mouse interaction events that capture screen coordinates c) Z-buffer algorithm.

coordinate system is expressed as follows:

$$\begin{bmatrix} X_c \\ Y_c \\ Z_c \\ 1 \end{bmatrix} = \begin{bmatrix} R & T \\ \vec{0} & 1 \end{bmatrix} \begin{bmatrix} X_w \\ Y_w \\ Z_w \\ 1 \end{bmatrix} \tag{1}$$

where R represents the rotation matrix; T represents the translation matrix; $P(X_w, Y_w, Z_w)$ represents the world coordinate system; $P(X_c, Y_c, Z_c)$ represents the camera coordinate system. The principle of perspective projection transformation for camera imaging is shown in Fig. 6-a, and the transformation process can be expressed as

$$Z_C \begin{bmatrix} x \\ y \\ 1 \end{bmatrix} = \begin{bmatrix} f & 0 & 0 & 0 \\ 0 & f & 0 & 0 \\ 0 & 0 & 1 & 0 \end{bmatrix} \begin{bmatrix} X_C \\ Y_C \\ Z_C \\ 1 \end{bmatrix} \tag{2}$$

where f represents the internal camera parameter; (x, y) is the pixel screen coordinate; Z_C represents the depth value. The mapping matrix P of pixel screen coordinates to world coordinates is

$$\mathrm{P} = \begin{bmatrix} \mathrm{f} & 0 & 0 & 0 \\ 0 & \mathrm{f} & 0 & 0 \\ 0 & 0 & 1 & 0 \end{bmatrix} \begin{bmatrix} \mathrm{R} & \mathrm{T} \\ \vec{0} & 1 \end{bmatrix} \tag{3}$$

It can be seen by equation (3) that the corresponding world coordinates can be solved by obtaining the pixel coordinates and depth values. Mouse interaction events can capture the screen pixel coordinates to acquire the information of the current imaging screen, as in Fig. 6-b.

As for the depth information, the model rendering environment is built in this paper and the depth value information is obtained by the Z-buffer algorithm. In dental model visualization, the mesh vertices are projected onto the screen according to the above projection matrix. However, these projections may overlap on the same pixel, so it is impossible to determine the occlusion relationship of the model. Therefore, the Z-buffer algorithm is introduced, as shown in Fig. 6-c, and the depth array Z-buffer (x, y) is maintained for the pixel points in the environment. The default depth value is set to infinitely far, traverse all the pixel points of the mesh patches, if the depth value of the pixel point is less than Z-buffer (x, y), update the depth value of the pixel point to the current pixel depth value to complete the rendering of a tooth model. Then, the current drawing point (2D) is mapped to the world coordinate system (3D) by the inverse transformation of the projection matrix, and then the boundary curve is fitted.

3) BOUNDARY CURVE PROJECTION OF PREPARATION AREA

The boundary curve of the preparation area cannot effectively fit the mesh surface after fitting, and part of the curve will pass through or float on the mesh surface, so the current curve cannot be used to segment the mesh model. The boundary curve needs to be projected onto the mesh patches section by section. The processing flow is shown in Fig. 7-a. Firstly, 200 sampling points were evenly sampled for the boundary curve of the preparation area; the sampling points are projected onto the tooth mesh surface to obtain the projection points. To not break the topological structure integrity of the mesh, the projection points are connected by a straight line. For the case that the projection points are distributed on different patches, it is necessary to solve the midpoint of the mesh patch to obtain the complete boundary curve on the mesh surface.

To solve the projection points on the tooth mesh surface: Find a point P' on the mesh surface so that the distance between the sampling point and projection point P' is minimum. Firstly, the KD tree divides the mesh space and finds the spatial region closest to the sampling point [29]. All mesh vertices in the region are traversed to find the closest mesh vertex N_i to the sampling point P. Predict that the projection point falls on a neighborhood patch of the mesh vertex N_i, find the closest distance to this neighborhood patch.

A vertical point on the neighborhood patch is found. According to the normal vector of the facet, the vector of the vertical point pointing to the sampling point multiplied by the normal vector point of the facet is 0. As shown in Fig. 7-b, according to the distribution of the vertical point on the patches: (a) The vertical point falls within the patch, that is, the vertical point is the projection point P'; (b) The vertical point falls outside the patch, the closest point to the vertical point on the triangular patch boundary is denoted as the projection point P'. Find the closest region from the projection point P' to the sampling point on a neighborhood patch of the mesh vertex N_i, and the index of the patch is denoted as the patch where the sampling point is projected, and P' is denoted as the projection point of the sampling point on the tooth mesh model.

The projection from the sampling points of the boundary curve to the tooth mesh surface was completed, according to the distribution of the projection points on the surface, including the two distribution types that projection points on the same surface and different surfaces, as shown in

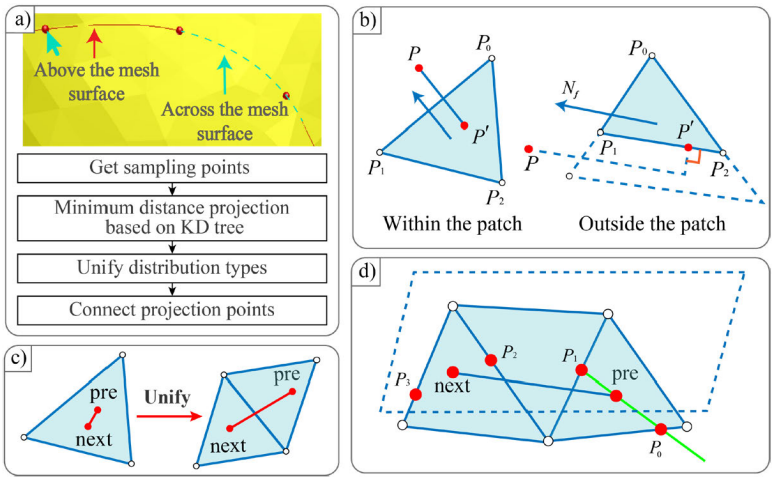

FIGURE 7. a) Preparation boundary projection and segmentation. b) Distribution of vertical points on the patches. c) Distribution of projection points on the patches. d) Solution of mesh boundary points.

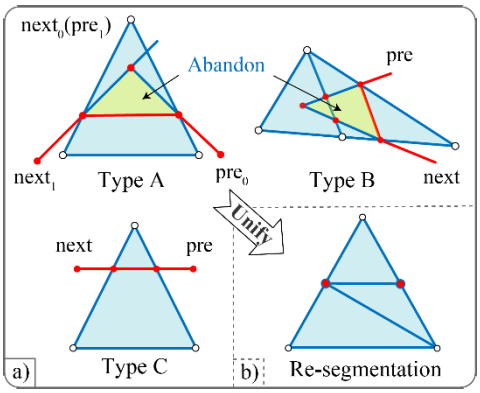

FIGURE 8. a) The type of patches that the boundary points passed through. b) Re-segmentation of patches.

Fig. 7-c. In order to maintain the integrity of the mesh topology and improve the efficiency of patches segmentation, one of the projection points will be abandoned when the next and previous projection points are distributed on the same triangular patch, so that each patch will distribute at most one projection point, that is, the distribution type is unified, and then all projection points are connected one by one. Since the triangle patches where the projection points are located are not in the same plane, the connection of projection points will pass through the mesh surface, so it is necessary to find the intermediate points on the boundary of the mesh patches, connect the projection point 'pre' with the mesh boundary point P_i, and connect the mesh boundary point P_i with the projection point 'next'. The solution of the mesh boundary point refers to the extraction method of the clipping curve. According to the point 'next', the point 'pre' and its patch normal vector, a construction plane is formed. The intersection of the triangle patch in the middle of the projection point and the construction plane is denoted as the mesh boundary point, as shown in Fig. 7-d.

4) ESTABLISH INNER AND OUTER BOUNDARY TO SEGMENT MODEL

In order to maintain the topological structure integrity of the tooth mesh model, it is necessary to re-segment the patches passed by the preparation boundary points and divide them into multiple triangle patches according to the counterclockwise order. Therefore, the analysis of the patches passed by the preparation boundary points can be divided into three categories, as shown in Fig. 8-a. (a) There are projection points on the passed patch, and the intersection lines between the projection plane and the patch are two straight lines; (b) All the same as (a) except the preparation boundary point is located on the same edge of the patch; (c) There is no projection point on the passed patch, and the passed patch is between a set of projection points. The preparation boundary point and the projection point of the patch are located on the projection plane, and the intersection line between the projection plane and the patch is straight.

In order to improve the margin smoothness of the preparation area after segmentation, the yellow area is abandoned, as shown in Fig. 8. Thereby three types of patches are converted into a uniform type. Since the number of selected patches is greater than 1000, the abandoned area accounts for the selected area less than 1 %, which has minimal impact on the shape of the overall selected area, and then re-segment the passed patches, as shown in Fig. 8-b. After reconstructing the topology structure of the patches, using the breadth-first traversal method, the preparation boundary points are inserted into the search queue Q as the search seed points, and the edge of the preparation boundary points are used as the inner and outer boundary to limit the search range of the traversal, as shown in Fig. 9-a.

The flow chart of breadth-first traversal is shown in Fig. 9-b. Through the vertex neighborhood relationship established, a neighborhood vertex of the seed point is accessed, and the neighborhood vertex of the boundary point is filtered. The unvisited neighborhood vertex is inserted into

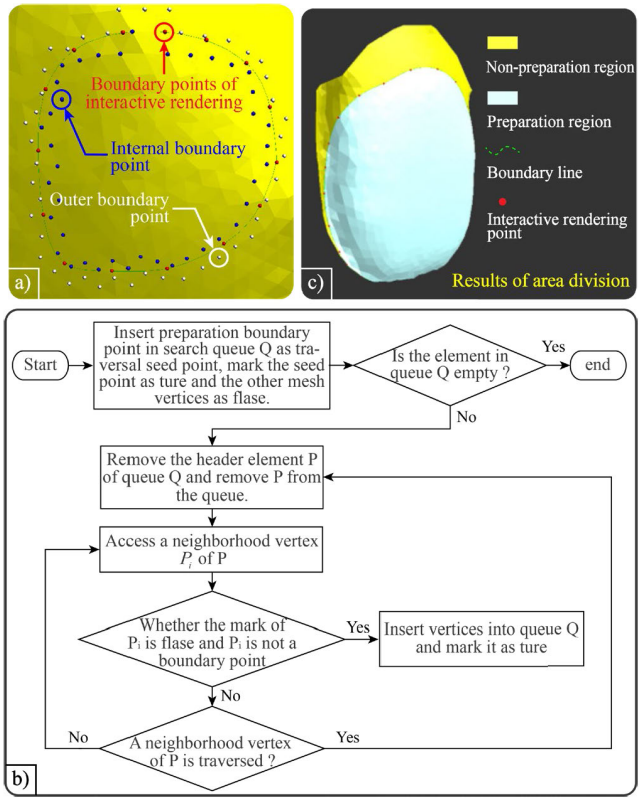

FIGURE 9. a) Determine inner and outer boundary points. b) Breadth-first traversal flow chart. c) Results of interactive selection of the preparatory region.

the search queue as a new seed point for searching. The mapping relationship with the original mesh is established, and the above cycle is repeated. Finally, the mesh vertex is divided into the inner and outer boundary areas. The inner boundary area is treated as the preparation area selected by the doctor, which is represented by blue mesh; The outer boundary region is denoted as a non-preparation area, which is represented by yellow mesh; Red spheres represent the boundary points selected by doctors, and the green line represents the boundary line of the preparation area based on boundary projection. As shown in Fig. 9-c, it provides a way for doctors to select the preparation area interactively.

5) PREPARATION AREA OFFSET AND PATCHES RESTORATION

In order to ensure that the prepared surface fits the natural tooth axis surface morphology, the design of the external surface of the preparation based on the replication idea is as follows: Obtain the optical scanning data; Meshing of surface data; The external surface of the preparation is obtained by offsetting the thickness of the restoration, and the offset distance is the preparation depth, which is set to the adjustable parameter. The offset based on the plane normal vector direction will produce more mesh self-intersections for the shrinkage offset. Therefore, the vertex normal vector is selected as the offset direction. The mesh vertices in the

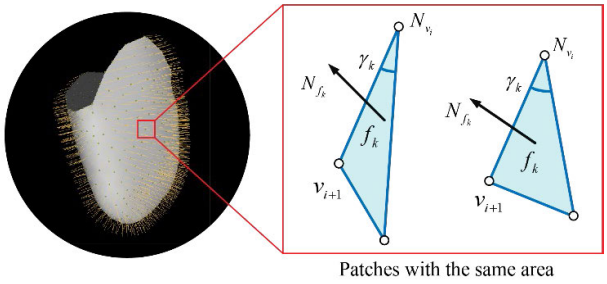

FIGURE 10. Normal vector estimation of grid vertices.

preparation area selected by the doctor are offset equidistantly along the normal direction of the vertex. Due to the discrete characteristics of the mesh model, there is no continuous normal vector and curvature, so it is necessary to estimate the normal vector of the mesh vertices. As shown in Fig. 10, the normal vectors generated by the patches with the same area but the obvious difference in shape are quite different.

In order to avoid the error generated in the offset as much as possible, the improved mesh vertex normal vector estimation method [30] is selected. This method takes into account the influence of the triangle patch shape of the mesh vertex neighborhood on the normal vector of the mesh vertex, so that the normal vector of the mesh vertex better represents the local characteristics of the neighborhood patch. The formula is as follows:

$$N_{v_i} = \frac{\sum_{f_k \in F^i} A_{f_k} \gamma_k N_{f_k}}{\left\| \sum_{f_k \in F^i} A_{f_k} \gamma_k N_{f_k} \right\|} \tag{4}$$

where N_{v_i} represents the normal vector of the mesh vertex v_i; f_k represents a neighborhood patch of the mesh vertex v_i; A_{f_k} represents the area of a neighborhood patch A_{f_k} of v_i; N_{f_k} represents the normal vector of f_k; F^i represents a neighborhood patch set of the grid vertex v_i; γ_k is the inner angle between a neighborhood patch f_k and the mesh vertex v_i.

Offset the mesh vertex along the normal vector of the vertex by a distance of 'preparation depth.' Considering the conservative principle of preparation, the preparation depth is parameterized, which can be used for doctors to make immediate adjustments according to the designed preparation model. The topology structure of the offset mesh is re-established, and the offset preparation area is shown in Fig. 11-a. The offset of the preparation area is a shrinking process, in which the mesh patches at the boundary appears folding and cusp phenomenon, which is due to the foldback of the boundary mesh vertex after offset along the normal vector direction. The fundamental reason is that there are problems in some normal vectors. No consideration is given to the effect of the shape of the triangular surface pieces of the mesh vertex neighborhood on the mesh vertex normal vectors. There is no continuous normal vector and curvature, and there are deviations from the real features.

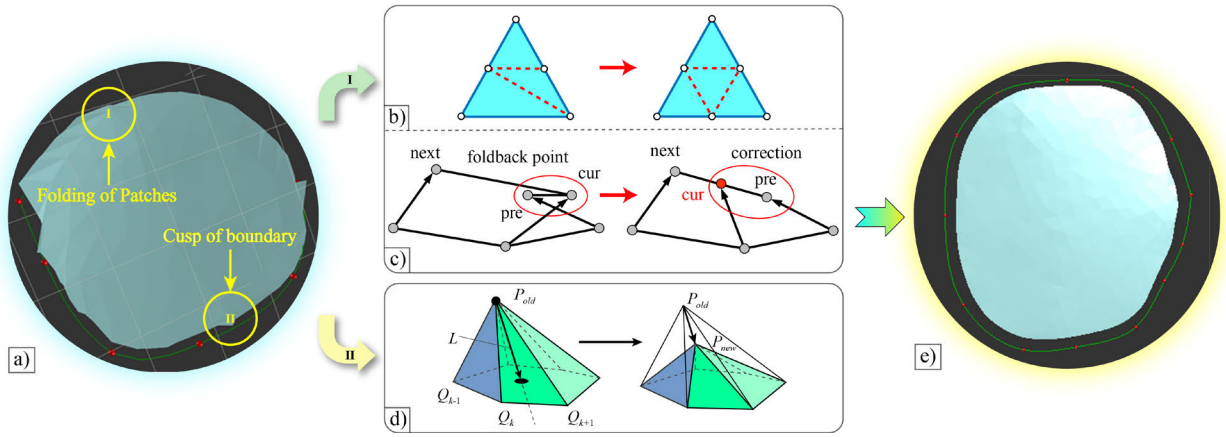

FIGURE 11. a) Preparation area before restoration. b) Re-segmentation of narrow triangular patches. c) Correction of boundary bias points. d) Laplacian smoothing principle. e) Preparation area after restoration.

(I) In this paper, a foldback point correction method based on secondary segmentation is proposed, including two steps: (1) When the boundary mesh patch is re-segmented, the narrow triangle patch generated by the previous segmentation method will interfere with the estimation of the normal vector of the vertex. Therefore, it is necessary to repair the narrow triangle, add a vertex to the patch and select the midpoint of the edge not crossed by the boundary in the patch as the new vertex, the mesh topology was reconstructed, as shown in Fig. 11-b. (2) The offset boundary vertices are corrected, and the mesh boundary points are traversed to detect the foldback point. When $(\mathbf{cur} - \mathbf{pre}) \cdot (\mathbf{next} - \mathbf{cur}) < 0$, 'cur' represents the foldback point, which is corrected to move the foldback point to the midpoint of the next and pre. This treatment is directly and efficiently, but the local deformation at the foldback point is large. With the idea of arc length parameterization, the local deformation of the foldback point is globally compensated. The distance between the boundary points is calculated, and all the boundary points are projected onto a circle with a radius of 1. According to the corrected distance of the foldback point, the parameter information on the arc is updated, mapped back to the boundary point and made corrections. The local deformation errors are equally distributed to the global, as shown in Fig. 11-c.

(II) Since the mesh vertices are not offset in the same direction, many cusps are found on the boundary of the offset mesh model, which destroys the smoothness of the boundary preparation area and affects the marginal adaptation of the preparation. Therefore, traverse all mesh boundary points, using the Laplacian smoothing [31] principle shown in Fig. 11-d to fix the cusps. The result is shown in Fig. 11-e.

The tooth mesh model is currently divided into preparation and non-preparation areas. There is a gap between the two areas, so mesh fusion is required for patching. As shown in Fig. 12, this paper extracts the boundaries of the two areas, establishes the boundary mapping relationship, stipulates that the vertex sequence of the triangle patches

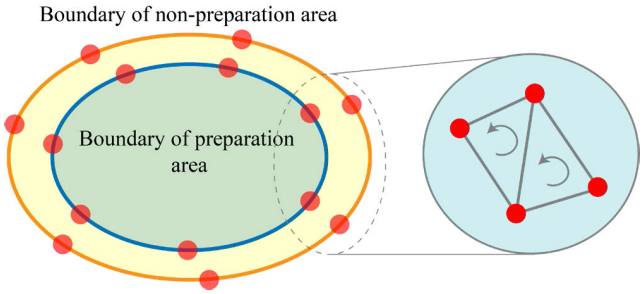

FIGURE 12. Patching the boundary of the preparation area.

is generated counterclockwise, the mesh topology sequence re-established, and the final preparation mesh model generated.

In order to better assist dentists in completing the interactive design of preparation morphology, based on the above algorithm, the interactive design software of the veneer preparation was developed. QT was used for the UI (User Interface) design of the software interface. Model rendering based on OpenGL and C++ as the underlying language. The UI interface of the interactive design system for the veneer preparation is shown in Fig. 4, which mainly includes the rendering parameter design module and the interactive design module. The functions of each part of the module are as follows.

a: RENDERING PARAMETER DESIGN MODULE

This module is used to set the parameters of the rendering environment, change the RGB value and transparency of the mesh model, add the point light source in the environment, and adjust the posture of the point light source and the ambient light variable. The configuration of environmental light variables and environmental parameters are based on the Phong illumination model. The above parameters are real-time controlled by buttons so that dentists can find suitable angles and parameters to improve the effect of tooth visualization.

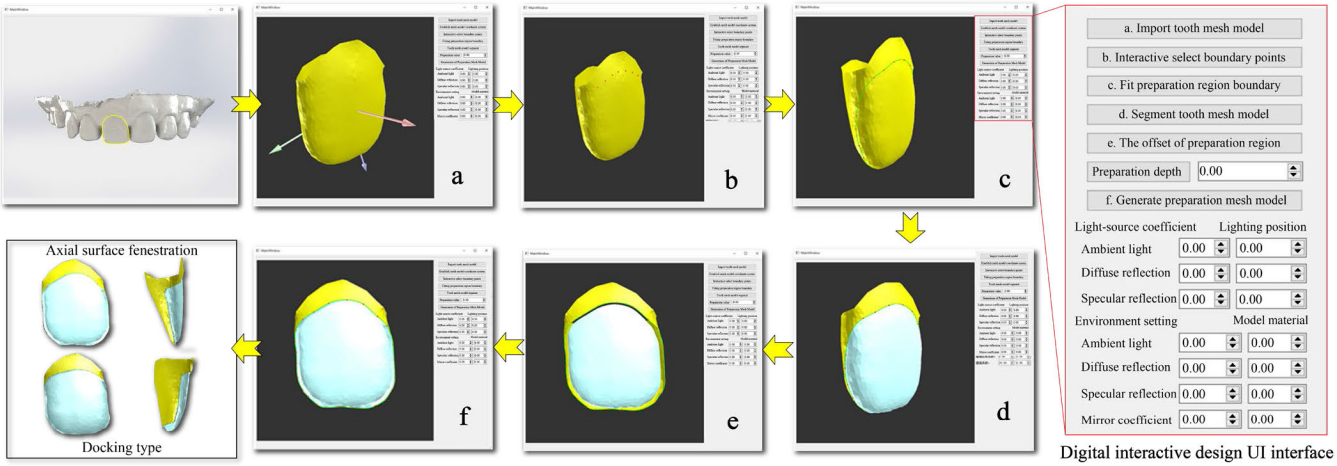

FIGURE 13. Digital interactive design system of veneer preparation.

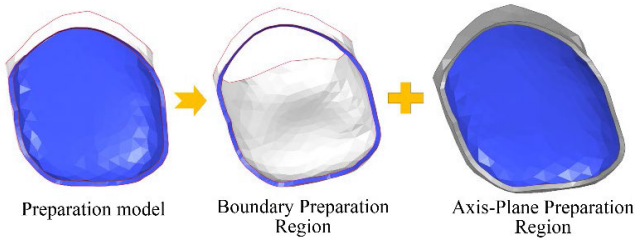

FIGURE 14. Schematic diagram of preparation area division.

b: INTERACTION DESIGN MODULE

This module mainly includes the following functions:

a. Import tooth mesh model: The imported tooth mesh model is inserted into the patch information, and a neighborhood structure of the vertex is established; the coordinate axis of the dental mesh model is fitted based on the PCA (Principal Component Analysis) algorithm. The covariance matrix is constructed, and the feature vector is decomposed. The minimum influence feature is used as the preparation feed direction selected by the dentist and expressed by the pink arrow.

b. Interactive select finishing lines points: Maintaining the depth buffer of the model to save the depth value, the dentist selects the pixels of the preparation area finishing lines through the mouse according to experience, obtain the screen coordinates and depth values, according to the inverse transformation of the projection matrix, the coordinate points of the model are inversed and displayed with red dots.

c. Fit preparation area finishing lines: The B-spline curve is fitted for the selected finishing lines points, the spline curve is decomposed and projected onto the mesh, the preparation finishing lines points between the projection points are solved, and the preparation finishing lines points are connected to obtain the finishing lines curve that effectively fits the mesh surface, which is represented by a green line.

d. Segment tooth mesh model: The patches passed by the preparation finishing lines are transformed into the same type, the mesh structure is re-segmented, and the inner and outer boundaries are established. Through breadth-first traversal, the mesh model is divided into the preparation area (blue) and the non-preparation area (yellow).

e. The offset of preparation area: Shrink offset is applied to the preparation area, and the preparation depth is parameterized for immediate adjustment by dentists.

f. Generate preparation mesh model: The gap of offset model is patched, the mesh topology sequence is reconstructed, and the final model is generated, which is used for robot trajectory planning of veneer preparation.

In this study, the central incisor was selected as the surface preparation object, and the tooth model was imported, and the morphology of the preparation was designed by the digital interactive design system of the veneer preparation. The axial surface fenestration and butt joint type of veneer preparation were selected for case analysis. The preparation models obtained by the interactive design are shown in Fig. 13.

III. ROBOT TRAJECTORY PLANNING OF VENEER PREPARATION

In order to facilitate the trajectory planning of the robot, according to the morphological characteristics of the fenestration preparation model, the model generated by the above interaction design system is divided into non-preparation area and preparation area. The preparation area is further divided into finishing lines preparation area and axial surface preparation area, as shown in Fig. 14. Since the adopted model format is STL, it is impossible to directly extract the corresponding three-dimensional curve for the veneer preparation model, so it is necessary to extract the discrete point sets on the model surface. These discrete point sets represent the characteristics of the veneer preparation model, and the preparation finishing lines and surface are obtained by fitting these discrete points, which are used for robot trajectory planning.

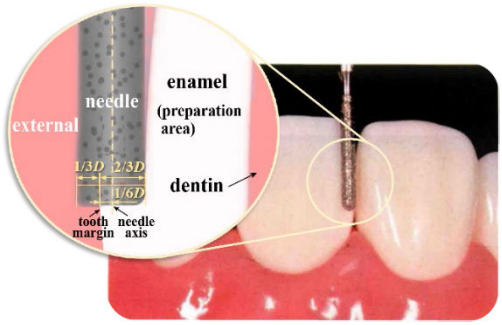

FIGURE 15. Position relationship between needle and tooth.

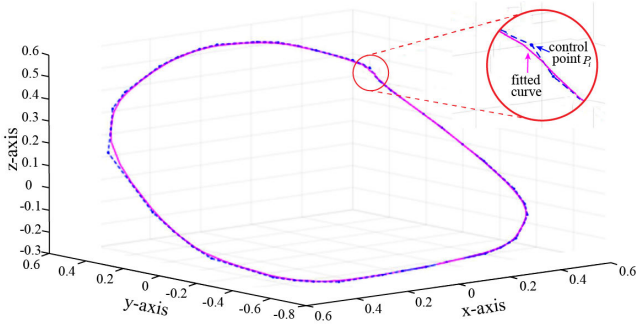

FIGURE 16. Fitting curve of robot end trajectory.

A. TRAJECTORY PLANNING OF FINISHING LINES PREPARATION AREA

To reserve the finishing allowance after processing, 0.45 mm is used as the maximum preparation depth, and the depth value is regarded as the width of the finishing lines preparation area. The diameter of the needle held at the robot end-effector is 1.2 mm. Supposing that the inner and outer contour of the finishing lines preparation area is selected as the planning target. When the needle grinds the outer contour of the finishing lines area, the maximum theoretical interference with the adjacent teeth is 0.6 mm, and the unexpected interference to the adjacent teeth must be avoided. When the needle exceeds the contour of the finishing lines area, it will cause interference and collision to the axial surface preparation area, destroy its smoothness, and directly affect the expected effect and service life of the veneer restoration. In summary, the end trajectory of the preparation finishing lines area is planned as a three-dimensional spatial curve, which considers the inner and outer contour constraints. The curve is as close as possible to the middle contour of the finishing lines preparation area.

Referring to the clinical tooth preparation guidelines [23], as shown in Fig. 15, the maximum theoretical interference distance between the needle and the adjacent tooth is controlled to 1/3 of the maximum needle diameter. During tooth preparation, the actual preparation area between the needle and the target tooth is only 2/3 of the needle diameter. Therefore, the finishing lines preparation area is transformed into a three-dimensional model with surface characteristics by using reverse engineering software, and the outer contour

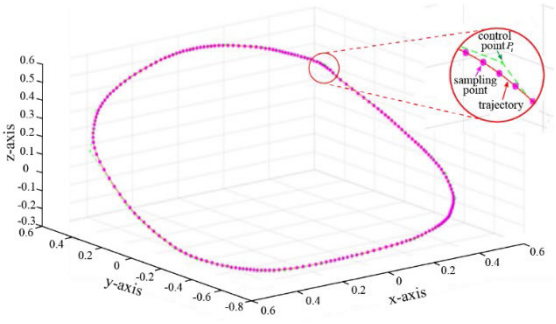

FIGURE 17. Sampling results of robot end trajectory.

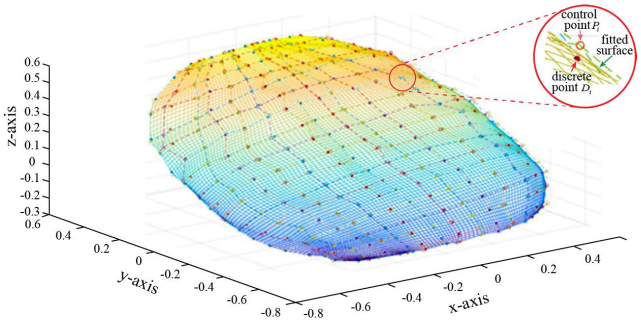

FIGURE 18. NURBS surface fitting results.

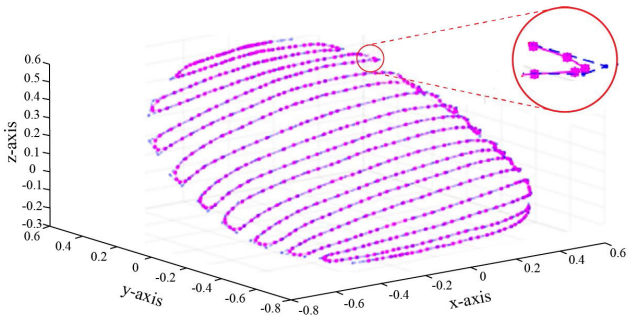

FIGURE 19. Sampling results of NURBS surface.

of the finishing lines preparation area is extracted. Then, the outer contour is offset by 1/6 needle diameter in the direction of the tooth center, and the ideal trajectory planning curve is obtained. The curve is output to get the discrete point Q. By using the method proposed in [24], the control point information P_i is inversed through the ideal trajectory planning curve, determines discrete points, node vectors, control points, and weight factors. The approximate original finishing lines preparation curve is obtained by B-spline curve fitting, and the fitting curve is shown in Fig. 16.

In the actual preparation process, considering the diameter of the needle and the operation of the robot joint steering gear, it is necessary to interpolate the fitting curve equation. By setting the time interval, the spatial points of the curve are segmented and sampled. The number of sampling points is 200, and the collection of sampling points is used as the end trajectory of the robot in the finishing lines preparation area, as shown in Fig. 17.

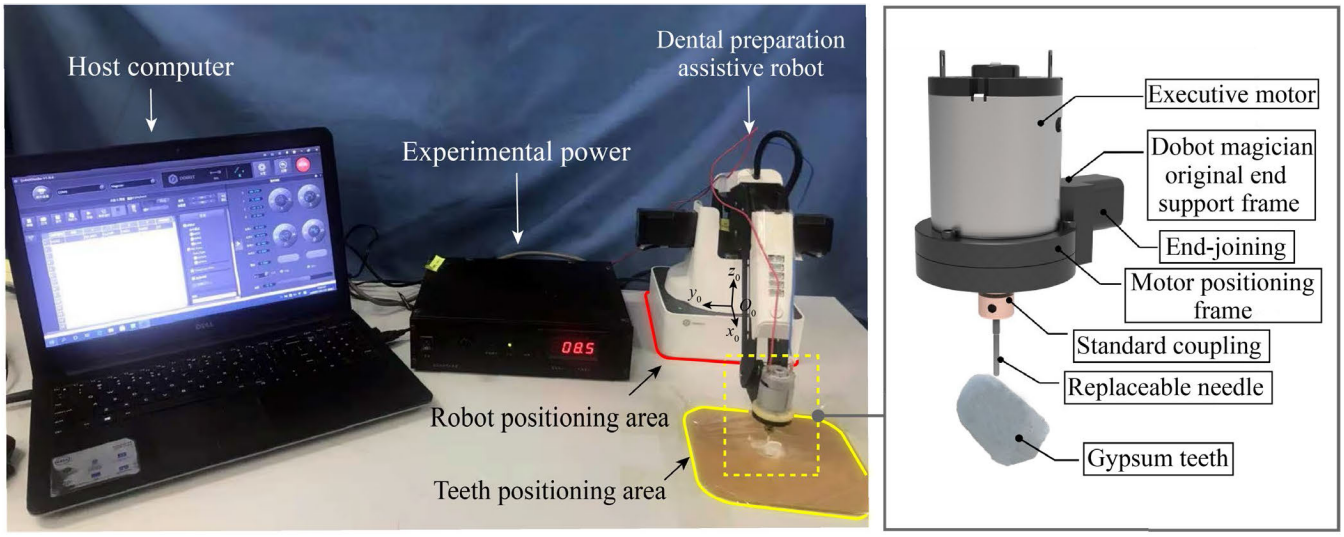

FIGURE 20. Experimental system of veneer preparation robot.

B. TRAJECTORY PLANNING OF AXIAL SURFACE PREPARATION AREA

The interpolation process is realized by MATLAB software. The NURBS surface fitting results of the axial surface preparation area are shown in Fig. 18. D_i is the input uneven mesh vertex. The power of input directions and directions is $p = q = 3$, the parameters in direction u and direction v are 16 and 19, and the number of control points P_i is 304.

After the control points of the surface are calculated, the robot end trajectory is fitted according to these control points of the surface. According to the isoparametric method, the u direction is chosen as the trajectory planning direction of the robot end, and the u direction is selected as the feed direction of the robot end to obtain the robot end trajectory. The obtained robot end trajectory needs to be sampled by setting the time interval $\{t_1, t_2, \ldots, t_k, \ldots, t_{n-1}, t_n\}$, the spatial points of the trajectory curve are segmented to obtain the set of data points with appropriate interval. The sampling results are shown in Fig. 19.

IV. ROBOT PREPARATION SYSTEM AND EXPERIMENTAL PROCESS

A. BUILDING OF EXPERIMENTAL SYSTEM

The serial joint manipulator of Dobot Magician is selected as the main body for the tooth preparation auxiliary robot, and its repeated positioning accuracy is 0.2 mm. The experimental system is built as shown in Fig. 20. The testing equipment consists of a testing power supply, tooth preparation robot prototype, and host computer.

B. EXPERIMENTAL PROCESS

The experimental object in this experiment was a STL model of the maxillary central incisor provided by the Second Hospital of Harbin Medical University (Heilongjiang Province, China). The original teeth model was obtained by 3D printing, and the original teeth model was used to make impressions and plaster perfusion to get the same proportion of plaster tooth model. Considering the irreversibility of the robot-assisted tooth preparation process, the preparation depth is decomposed into 0.15 mm, 0.3 mm, and 0.45 mm. The model is planned and generated layer by layer to facilitate dentists to make real-time control and reserve some refinement space. The robot layering trajectory is shown in Fig. 21.

The planned trajectory points and tooth model are matrix-transformed to make the gum side close to the x-o-y plane, facilitate the stable placement of gypsum teeth, and ensure the processing space. The pose relationship between the tooth and the robot is established by the method proposed in [24] and [25], and the pose relationship between them is calibrated. The coordinate centers of the robot positioning area and the tooth positioning (acrylic plate) area are determined. The plaster tooth is fixed on the acrylic plate, and the acrylic plate is set on the worktable by bonding. The standard axial surface preparation needle was selected during the experiment. The needle head was a curved surface with a diameter of 1.2 mm. The experimental voltage was 12 V, the current was 0.25 A, the end speed was about 46000 r/min, and the robot moving speed was 12 mm/s, which was 10 % of the setting storage point playback speed. The experimental process of robot preparation is shown in Fig. 22.

V. RESULTS

Accuracy analysis of veneer preparation based on the team's previous method of post-preparation analysis of full crowns [24], [25]. The selection of the feature points of veneer preparation is shown in Fig. 22, and three pairs of feature points A, B, C, D, E, and F, which are symmetrically distributed on the three sides of the preparation finishing lines area, are extracted to analyze the preparation depth of the

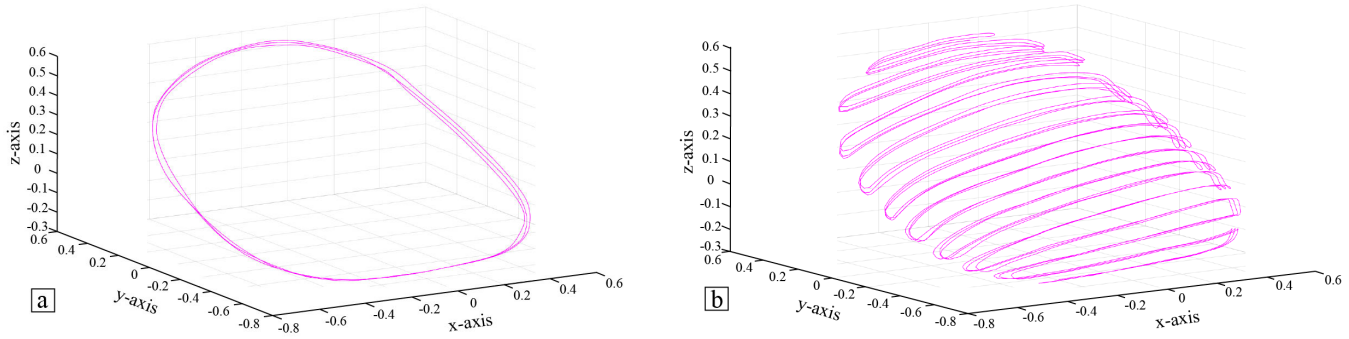

FIGURE 21. a) Layered trajectory of finishing lines preparation area. b) Layered trajectory of axial surface preparation area.

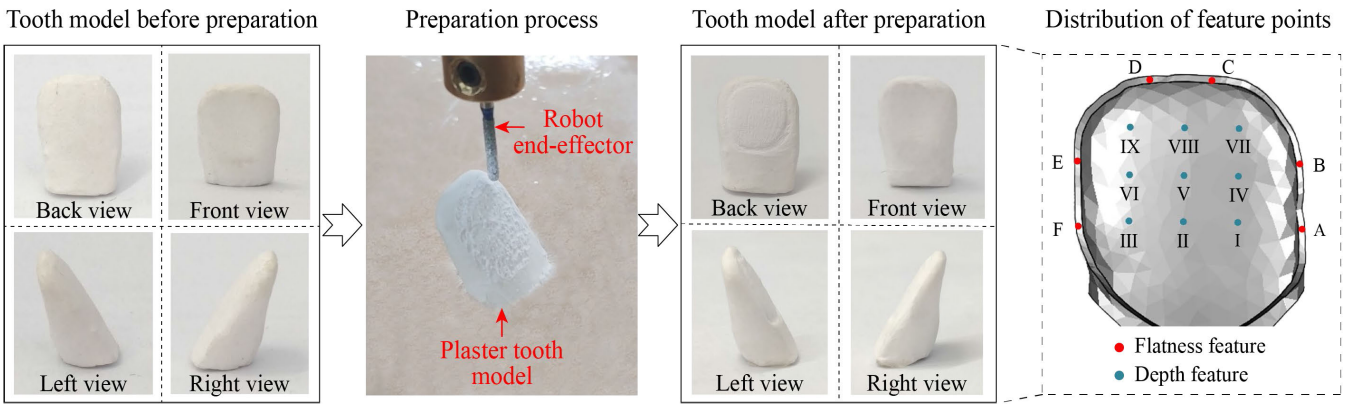

FIGURE 22. Experimental process and feature points division of robot-assisted veneer preparation.

processed model. Nine equidistant feature points I, II, III, IV, V, VI, VII, VIII, and IX arranged squarely in the axial surface area were extracted to analyze the surface flatness of the processed model. The experimental accuracy of the robot-assisted preparation is verified by comparing the extracted actual feature points with the feature points of the designed mesh model. The theoretical values of the preparation feature points are shown in Table 1.

According to the position of feature points in the interpolation curve, the preparation completed by the robot is marked and measured. In the measurement process, the relative position between the gypsum tooth and the robot is ensured to be the same as that in the process stage. The feature points marked on the plaster tooth are measured by the robot teaching mode. The reading begins when the head of the needle is fully fitted with the feature point. The teaching measurement accuracy can be regarded as the repeated positioning accuracy of 0.2 mm. Five times are measured and recorded at each point, then multiplied by the transformational matrix. A total of 50 experimental data points were obtained, shown in Table 2 and Table 3.

VI. DISCUSSIONS

A. EXPERIMENTAL DATA ANALYSIS

The experimental value and theoretical value of the collected feature points are calculated and analyzed from the three coordinate directions of X, Y and Z, respectively. The errors include systematic error and random error. Among them, the system error is composed of several error factors with deterministic variation. In this paper, the finishing lines of system error is defined by mean μ, sample standard deviation s and the confidence interval $[\bar{x} - k_1 s, \bar{x} + k_1 s]$ of mean μ of measurement, where $\bar{x}$ is the unbiased estimator of μ, and the safety factor k_1 is determined by the percentage of the confidence interval. In addition, the relative error indexes in three directions of XYZ were evaluated by relative-fixed point error ε and relative standard deviation (RSD).

Taking the x-axis coordinate value of feature point A as an example, the relative fixed-point error ε_A^x is the error of the mean of measurement relative to the theoretical value. The expression is:

$$\varepsilon_A^x = |\bar{x}_A - x_A| \tag{5}$$

where: $\bar{x}_A = \sum x_{A-i}/n$; x_{A-i} is the i-th measurement value of x-axis of feature point A; x_A is the x-axis theoretical value of feature point A in Table 1.

Standard deviation RSD can be used to test the precision of the measurement results, the expression is:

$$RSD_A^x = \frac{s_A}{\bar{x}_A} \times 100\% \tag{6}$$

TABLE 1. Feature points theoretical values of veneer preparation.

Reference point	Feature Points of Preparation Depth					
Coordinate	A	B	C	D	E	F
x/mm	-0.84	-0.84	-0.28	0.49	0.09	0.21
y/mm	0.56	0.45	-0.49	-0.39	0.25	0.54
z/mm	0.89	0.78	-0.18	0.28	0.68	0.86

Reference point	Feature Points of Preparation Flatness								
Coordinate	I	II	III	IV	V	VI	VII	VIII	IX
x/mm	-0.85	-0.50	-0.46	-1.15	-0.75	-0.35	-1.15	-0.74	-0.20
y/mm	0.75	0.82	0.72	0.89	0.75	0.69	0.46	0.52	0.68
z/mm	0.99	1.11	1.02	1.57	1.35	1.47	1.15	1.05	1.55

TABLE 2. Feature points actual values of preparation depth.

Times / Feature point	First measurement	Second measurement	Third measurement	Fourth measurement	Fifth measurement
A	(-0.94, 0.47, 0.73)	(-0.85, 0.62, 0.75)	(-0.84, 0.53, 0.73)	(-0.84, 0.59, 0.80)	(-0.86, 0.55, 0.74)
B	(-0.79, 0.47, 0.76)	(-0.82, 0.45, 0.73)	(-0.81, 0.42, 0.68)	(-0.79, 0.43, 0.73)	(-0.75, 0.30, 0.64)
C	(-0.37, -0.47, -0.22)	(-0.23, -0.49, -0.16)	(-0.25, -0.41, -0.11)	(-0.26, -0.55, -0.23)	(-0.30, -0.48,-0.20)
D	(0.50, -0.32, 0.32)	(0.49, -0.32, 0.34)	(0.48, -0.42, 0.28)	(0.48, -0.38, 0.33)	(0.45, -0.40, 0.26)
E	(0.20, 0.21, 0.89)	(0.29, 0.16, 0.73)	(0.27, 0.15, 0.70)	(0.29, 0.14, 0.72)	(0.30, 0.24, 0.88)
F	(0.21, 0.47, 0.83)	(0.19, 0.47, 0.81)	(0.20,0.49, 0.83)	(0.21, 0.55, 0.91)	(0.19, 0.59, 0.95)

TABLE 3. Feature points actual values of preparation flatness.

Times / Feature point	First measurement	Second measurement	Third measurement	Fourth measurement	Fifth measurement
I	(-0.86, 0.72, 0.97)	(-0.83, 0.71, 0.95)	(-0.83, 0.79, 1.03)	(-0.87, 0.83, 1.09)	(-0.87, 0.67, 0.90)
II	(-0.47, 0.82, 1.23)	(-0.50, 0.78, 1.17)	(-0.51, 0.75, 1.11)	(-0.52, 0.81, 1.22)	(-0.46, 0.73, 1.11)
III	(-0.45, 0.79, 1.04)	(-0.44, 0.74, 1.14)	(-0.44, 0.72, 1.12)	(-0.44, 0.72, 1.09)	(-0.44, 0.73, 1.13)
IV	(-1.09, 1.05, 1.38)	(-0.92, 0.93, 1.48)	(-1.06, 1.06, 1.54)	(-1.12, 0.98, 1.43)	(-1.11, 0.95, 1.43)
V	(-0.74, 0.80, 1.32)	(-0.71, 0.81, 1.38)	(-0.71, 0.80, 1.37)	(-0.72, 0.70, 1.31)	(-0.74, 0.88, 1.31)
VI	(-0.39, 0.67, 1.35)	(-0.30, 0.73, 1.42)	(-0.33, 0.78, 1.45)	(-0.29, 0.60, 1.31)	(-0.34, 0.78, 1.55)
VII	(-1.03, 0.53, 1.03)	(-1.04, 0.57, 1.08)	(-1.03, 0.54, 1.02)	(-1.05, 0.48, 0.94)	(-1.00, 0.40, 0.97)
VIII	(-0.64, 0.44, 1.06)	(-0.67, 0.53, 1.09)	(-0.62, 0.47, 1.09)	(-0.67, 0.58, 1.12)	(-0.65, 0.43, 0.85)
IX	(-0.35, 0.71, 1.51)	(-0.39, 0.66, 1.37)	(-0.28, 0.74, 1.49)	(-0.36, 0.76, 1.56)	(-0.35, 0.63, 1.41)

where, s_A is the sample standard deviation of characteristic point A,

$$s_A = \sqrt{\frac{1}{n-1}\sum_{i=1}^{n}(x_{A-i} - \bar{x}_A)^2} \tag{7}$$

The confidence is selected as 95%, and the value of the safety factor k_1 is determined to be 2.132 according to the t-distribution quantile table. The error parameters of the calculated experimental data are shown in Table 4 and Table 5.

It can be seen from Table 4 and Table 5 that the relative fixed-point errors ε of the feature points in the directions of X, Y and Z are 0.002∼0.18, 0.008∼0.036 and 0.006∼0.14 mm, respectively. The error of the feature points is controlled within 0.3 mm. The robot can accurately reach each feature point in the two regions in the surface preparation. The relative fixed-point error e ranges of flatness feature points in X, Y and Z directions are 0.002∼0.146, 0.006∼0.104 and 0.002∼0.142 mm, respectively. In terms of RSD, the relative standard error of the preparation depth feature points is larger than that of the flatness feature points on the whole. The reason is that the preparation depth feature points are distributed at the margin of the tooth, so the measurement is difficult. The relative standard error of X direction in preparation depth characteristic points A, B, C, D, E and F was 3.39%∼10.44%, 10.42%∼23.90% in Y direction and 3.89%∼13.24% in Z direction. The relative standard error of X direction is 1.01%∼11.93%, Y direction is 3.94%∼13.21%, Z direction is 2.56 %∼10.50% in I, II, III, IV, V, VI, VII, VIII, IX; the confidence interval widths of each feature point in X, Y and Z directions are 0.02∼0.35, 0.12∼0.60 and 0.11∼0.40 mm, respectively. The width of the confidence interval in different directions under the same feature point is stable at about 0.3 mm on average, which shows that the system error of each feature point in veneer preparation is stable in a small range, which verifies the correctness of the tooth preparation trajectory

TABLE 4. Statistical table of system error parameters of preparation depth feature points.

Direction	Parameters	Feature Points					
		A	B	C	D	E	F
X-Direction	μ /mm	-0.866	-0.792	-0.282	0.480	0.270	0.200
	ε /mm	0.026	0.048	0.002	0.010	0.180	0.010
	RSD/%	4.87	3.39	10.44	3.90	4.66	5.00
	Confidence interval	[-0.955, -0.776]	[-0.849, -0.734]	[-0.344, -0.219]	[0.440, 0.520]	[0.243, 0.297]	[0.179, 0.221]
Y-Direction	μ /mm	0.552	0.414	-0.480	-0.368	0.180	0.514
	ε /mm	0.008	0.036	0.010	0.022	0.070	0.026
	RSD/%	10.44	16.08	10.42	12.51	23.90	10.44
	Confidence interval	[0.429, 0.675]	[0.272, 0.556]	[-0.586, -0.373]	[-0.466, -0.269]	[0.088, 0.272]	[0.400, 0.628]
Z-Direction	μ /mm	0.75	0.708	-0.204	0.306	0.784	0.866
	ε /mm	0.14	0.072	0.024	0.026	0.104	0.006
	RSD/%	3.89	6.73	13.24	11.23	11.85	7.01
	Confidence interval	[0.688, 0.812]	[0.606, 0.810]	[-0.261, -0.146]	[0.233, 0.379]	[0.586, 0.982]	[0.737, 0.995]

TABLE 5. Statistical table of system error parameters of preparation flatness feature points.

Direction	Parameters	I	II	III	IV
X-Direction	μ /mm	-0.852	-0.492	-0.442	-1.060
	ε /mm	0.002	0.008	0.018	0.090
	RSD/%	2.41	5.26	1.01	7.693
	Confidence interval	[-0.895, -0.808]	[-0.547, -0.436]	[-0.451, -0.432]	[-1.233, -0.886]
Y-Direction	μ /mm	0.744	0.778	0.740	0.994
	ε /mm	0.006	0.042	0.020	0.104
	RSD/%	8.69	4.93	3.94	5.89
	Confidence interval	[0.606, 0.882]	[0.696, 0.860]	[0.678, 0.802]	[0.869, 1.119]
Z-Direction	μ /mm	0.988	1.168	1.104	1.452
	ε /mm	0.002	0.058	0.084	0.118
	RSD/%	7.45	4.93	3.66	4.17
	Confidence interval	[0.831, 1.145]	[1.045, 1.291]	[1.018, 1.190]	[1.323, 1.581]

		V	VI	VII	VIII	IX
X-Direction	μ /mm	-0.724	-0.330	-1.030	-0.650	-0.346
	ε /mm	0.026	0.020	0.120	0.090	0.146
	RSD/%	2.095	11.93	1.82	3.26	11.67
	Confidence interval	[-0.756, -0.691]	[-0.413, -0.246]	[-1.069, -0.990]	[-0.695, -0.604]	[-0.432, -0.259]
Y-Direction	μ /mm	0.798	0.712	0.504	0.490	0.7
	ε /mm	0.048	0.022	0.044	0.030	0.020
	RSD/%	8.04	10.85	13.21	12.99	7.76
	Confidence interval	[0.661, 0.935]	[0.547, 0.877]	[0.362, 0.646]	[0.354, 0.626]	[0.584, 0.816]
Z-Direction	μ /mm	1.338	1.416	1.008	1.042	1.468
	ε /mm	0.012	0.054	0.142	0.008	0.082
	RSD/%	2.56	6.58	5.41	10.50	5.24
	Confidence interval	[1.265, 1.411]	[1.217, 1.615]	[0.892, 1.124]	[0.809, 1.275]	[1.304, 1.632]

planning method and the feasibility of robot assisted dentist to complete tooth preparation.

B. DEFICIENCIES AND ADVANTAGES OF THE SYSTEM

Of course, there are still some limitations in this study. First, for the reproducibility of the experiment, the team's previous research method of choosing a plaster model was continued. The plaster model is characterized by small deformation, high plasticity and easy processing, and although there is a hardness difference between it and the real tooth, it can still simulate the directional removal of material from the real tooth. The feasibility of this system can be continued to be verified on the isolated tooth later. Secondly, the repeat positioning accuracy of the robot selected for this experiment

is 0.2 mm, which is slightly lower than other robots used in dental prosthetics, but the feasibility of the system is still verified by this experimental study. A robot with higher accuracy can be used later to further validate the system. Finally, the target teeth used in this study are the patient teeth provided by the collaborative unit, and the designed system is a tooth-specific algorithm, which is not universal. However, the studied algorithm and designed system can still be a reference for future researchers interested in this research content. The system will be enriched with a library of relevant preparations [32] based on the parameters of different teeth.

VII. CONCLUSION

This paper presents a digital interactive design system for tooth veneer preparation. Taking fenestration preparation as an example, the overall scheme is determined according to the preparation requirements and operation process. Firstly, to simplify the tooth mesh model and improve the storage form of patches, this paper proposes to use point drawing to interactively select the preparation area, and the minimum distance projection method is used to obtain the effective finishing lines curve. Then the breadth-first traversal method is used to divide the model into the preparation and the non-preparation area. The foldback point correction method based on secondary segmentation is used to repair the offset preparation area. Finally, the digital interactive design system is built and the required preparation model are generated. The model is divided into two feature areas which are interpolated based on B-spline curve and NURBS surface, respectively. The isoparametric curve method is used to plan the preparation trajectory. The physical prototype of the veneer preparation robot is built and the preparation experiment is carried out. The error of the feature points of the preparation depth is 0.002∼0.180 mm, 0.008∼0.036 mm, 0.006∼0.140 mm in the three directions of X, Y, and Z, respectively. The error of the feature points of the flatness is 0.002∼0.146 mm, 0.006∼0.104 mm, 0.002∼0.142 mm in the three directions of X, Y, and Z, respectively. The average confidence interval width of the system error is stable at about 0.3 mm. The results show that the feasibility of the digital interactive design system. Based on the proposed tooth preparation trajectory planning method, the robot can be prepared in an acceptable error range.

In the future, we plan to continue to expand the digital interactive design system for the complete crown preparation, improve its design and interaction, and try to apply robot-assisted tooth preparation to the mouth with higher precision robot. In addition, the system can be further developed for the simulation teaching of new dentists, digital demonstration and the effect evaluation of the designed preparation model.

REFERENCES

[1] C. D'Arcangelo, M. Vadini, M. D'Amario, Z. Chiavaroli, and F. Angelis, "Protocol for a new concept of no-prep ultrathin ceramic veneers," *J. Esthetic Restorative Dentistry*, vol. 30, no. 3, pp. 1–7, Jun. 2017.

[2] J. Jiang, Z. Huang, X. Ma, Y. Zhang, T. He, and Y. Liu, "Establishment and experiment of utility archwire dynamic orthodontic moment prediction model," *IEEE Trans. Biomed. Eng.*, vol. 67, no. 7, pp. 1958–1968, Jul. 2020.

[3] M. Gresnigt and M. Ozcan, "Esthetic rehabilitation of anterior teeth with porcelain laminates and sectional veneers," *J. Can. Dental Assoc.*, vol. 77, pp. 1–8, Dec. 2011.

[4] Z. Sun, L. Wu, J. Zhao, and Y. Zheng, "Aesthetic restoration of anterior teeth with different coloured substrates using digital monolithic zirconia crowns: Two case reports," *Adv. Appl. Ceram.*, vol. 120, no. 3, pp. 1–6. Apr. 2021.

[5] M. Özcan, C. A. M. Volpato, and L. G. D. Garbelotto, "Esthetic and functional rehabilitation of worn teeth," *Clin. Dentistry Reviewed*, vol. 5, no. 1, pp. 1–13, Dec. 2021.

[6] R. Sharma, V. Hegde, M. Siddharth, R. Hegde, G. Manchanda, and P. Agarwal, "Endodontic-periodontal microsurgery for combined endodontic-periodontal lesions: An overview," *J. Conservative Dentistry*, vol. 17, no. 6, pp. 510–516, Nov. 2014.

[7] N. Dai, Y. Zhong, H. Liu, F. Yuan, and Y. Sun, "Digital modeling technology for full dental crown tooth preparation," *Comput. Biol. Med.*, vol. 71, pp. 190–197, Apr. 2016.

[8] L. F. Da Cunha, L. O. Pedroche, C. C. Gonzaga, and A. Y. Furuse, "Esthetic, occlusal, and periodontal rehabilitation of anterior teeth with minimum thickness porcelain laminate veneers," *J. Prosthetic Dentistry*, vol. 112, no. 6, pp. 1315–1318, Dec. 2014.

[9] F. N. Arcelino, C. D. M. Fernanda, V. Larissa, and S. C. Mariana, "Tooth preparation for ceramic veneers: When less is more," *Int. J. Esthetic Dentistry*, vol. 14, no. 2, pp. 156–164. 2019.

[10] F. Yuan, Y. Sun, Y. Wang, and P. Lv, "Computer-aided design of tooth preparations for automated development of fixed prosthodontics," *Comput. Biol. Med.*, vol. 44, pp. 10–14, Jan. 2014.

[11] A. Zeller, R. M. Zimmerer, S. Springhetti, F. Tavassol, B. Rahlf, M. Neuhaus, and N. Gellrich, "CAD/CAM-based referencing aids to reduce preoperative radiation exposure for intraoperative navigation," *Int. J. Med. Robot. Comput. Assist. Surgery*, vol. 17, no. 3, p. e2241, Mar. 2021.

[12] A. H. Kamali, M. Moradi, F. Goodarzian, and P. Ghasemi, "A discrete event simulation method for performance analysis of an additive manufacturing in the dental clinic," *Int. J. Adv. Manuf. Technol.*, vol. 118, nos. 9–10, pp. 2949–2979, Oct. 2021.

[13] S. M. D. L. Gontijo, P. M. Morgado, L. S. Neves, E. C. França, E. M. B. Lages, and H. H. Alvim, "Digital smile design as a tool in the planning of porcelain laminate veneers restoration," *Revista Gaúcha de Odontologia*, vol. 69, no. s1, 2021, Art. no. e20210019.

[14] J. Gao, J. Li, C. Liu, F. Lin, J. Yu, and H. Yu, "A stereolithographic template for computer-assisted teeth preparation in dental esthetic ceramic veneer treatment," *J. Esthetic Restorative Dentistry*, vol. 32, no. 6, pp. 1–7, 2020.

[15] P. Silva, K. Stanley, and J. Gardee, "Laminate veneers: Preplanning and treatment using digital guided tooth preparation," *J. Esthetic Restorative Dentistry*, vol. 32, no. 7, pp. 1–11. Mar. 2020.

[16] M. Eugster, J.-P. Merlet, N. Gerig, P. C. Cattin, and G. Rauter, "Miniature parallel robot with submillimeter positioning accuracy for minimally invasive laser osteotomy," *Robotica*, vol. 40, no. 4, pp. 1070–1097, Apr. 2022.

[17] C.-S. Tseng, C.-C. Huang, and C.-S. Chen, "Development of an image-guided robotic system for surgical positioning and drilling," *Robotica*, vol. 25, no. 3, pp. 375–383, May 2007.

[18] T. Kan, K. Cheng, Y. Liu, R. Wang, W. Zhu, F. Zhu, X. Jiang, and X. Dong, "Evaluation of a custom-designed human–robot collaboration control system for dental implant robot," *Int. J. Med. Robot. Comput. Assist. Surg.*, vol. 18, no. 1, p. e2346, Nov. 2021.

[19] J. Li, Z. Shen, W. Y. T. Xu, W. Y. H. Lam, R. T. C. Hsung, E. H. N. Pow, K. Kosuge, and Z. Wang, "A compact dental robotic system using soft bracing technique," *IEEE Robot. Autom. Lett.*, vol. 4, no. 2, pp. 1271–1278, Apr. 2019.

[20] T. Otani, A. J. Raigrodski, L. Mancl, I. Kanuma, and J. Rosen, "In vitro evaluation of accuracy and precision of automated robotic tooth preparation system for porcelain laminate veneers," *J. Prosthetic Dentistry*, vol. 114, no. 2, pp. 229–235, Aug. 2015.

[21] F. Yuan, Y. Wang, Y. Zhang, Y. Sun, D. Wang, and P. Lyu, "An automatic tooth preparation technique: A preliminary study," *Sci. Rep.*, vol. 6, no. 1, p. 25281, Apr. 2016.

[22] F. Yuan and P. Lyu, "A preliminary study on a tooth preparation robot," *Adv. Appl. Ceram.*, vol. 119, nos. 5–6, pp. 332–337, Sep. 2019.

[23] M. A. Z. Loureiro, M. R. A. Elias, L. R. Capeletti, J. A. Silva, P. C. Siqueira, G. S. Chaves, and D. A. Decurcio, "Guided endodontics: Volume of dental tissue removed by guided access cavity preparation—An ex vivo study," *J. Endodontics*, vol. 46, no. 12, pp. 1907–1912, Dec. 2020.
[24] J. G. Jiang, J. Sun, Y. Zeng, Y. Zhang, J. Wang, and S. Zhou, "Determination of vibration acceleration mechanism and vibration load application duration from a non-biological perspective: Orthodontic acceleration," *Latin Amer. J. Solids Struct.*, vol. 20, no. 1, p. e474, Jan. 2023.
[25] J. Jiang, Y. Guo, Z. Huang, Y. Zhang, D. Wu, and Y. Liu, "Adjacent surface trajectory planning of robot-assisted tooth preparation based on augmented reality," *Eng. Sci. Technol., Int. J.*, vol. 27, Mar. 2022, Art. no. 101001.
[26] M. Chen, B. Tu, and B. Lu, "Triangulated manifold meshing method preserving molecular surface topology," *J. Mol. Graph. Model.*, vol. 38, pp. 411–418, Sep. 2012.
[27] M. Wang, J. Gao, and X. Wang, "High-quality mesh generation for human hip based on ideal element size: Methods and evaluation," *Comput. Assist. Surgery*, vol. 22, no. sup1, pp. 212–220, Oct. 2017.
[28] B. Zhang, N. Dai, S. Tian, F. Yuan, and Q. Yu, "The extraction method of tooth preparation margin line based on S-Octree CNN," *Int. J. Numer. Methods Biomed. Eng.*, vol. 35, no. 10, p. e3241, Oct. 2019.
[29] Y. Zhao, Y. Wang, J. Zhang, C.-W. Fu, M. Xu, and D. Moritz, "KD-Box: Line-segment-based KD-tree for interactive exploration of large-scale time-series data," *IEEE Trans. Vis. Comput. Graph.*, vol. 28, no. 1, pp. 890–900, Jan. 2022.
[30] H. Shen, J. Li, and L. Zhou, "Estimation of triangular mesh vertex normal vector and discrete curvature," *Comput. Eng. Appl.*, vol. 41, pp. 12–15, Sep. 2005.
[31] J. Hu, B. Liu, C. Huang, and K. Jiang, "Interactive pattern design of freeform features on mesh surface," *Comput. Integr. Manuf. Syst.*, vol. 25, pp. 61–70, Jan. 2019.
[32] J. Jiang, J. Sun, Z. Huang, Z. Bi, G. Yu, J. Yang, and Y. Wang, "The state of the art and future trends of root canal files from the perspective of patent analysis: A study design," *Biomed. Eng. Online*, vol. 21, no. 1, p. 90, Dec. 2022.

SUN JIAN-PENG was born in Heilongjiang, China, in 1998. He received the B.S. degree from the Harbin University of Science and Technology, where he is currently pursuing the doctoral degree in mechanical engineering. He is currently working on medical device materials. His current research interests include dental materials and dental instrument materials.

JIANG JIN-GANG (Member, IEEE) received the B.Sc., M.Sc., and Ph.D. degrees from the Harbin University of Science and Technology, in 2005, 2008, and 2013, respectively. Currently, he is a Professor and a Doctoral Supervisor with the Harbin University of Science and Technology. His main research interests include medical robots and biomimetic robots.

QIAN WEI received the B.Sc. and M.Sc. degrees from the Harbin University of Science and Technology, in 2018 and 2021, respectively. His main research interests include medical robots and medical image processing.

HUANG ZHI-YUAN was born in Heilongjiang, China, in 1995. He received the B.S. and M.S. degrees from the Harbin University of Science and Technology, in 2017 and 2020, respectively. He is currently pursuing the Ph.D. degree with the State Key Laboratory of Robotics and Systems, Harbin Institute of Technology. His current research interests include augmented reality and microfabrication.

MA HONG-YUAN was born in Heilongjiang, China. He is currently a Technician with the China Electronics Technology Group Corporation and is well-versed in robotic communication systems and medical robotics. In particular, he is interested in the application of dental robots in dental preparation.

ZHOU SHAN is the Director of the Department of Orthodontics, Second Hospital of Harbin Medical University. He is also the Chief Physician and the Doctor of dental medicine. He is currently a member of the Orthodontic Committee, Chinese Medical Association; the Deputy Director of the Orthodontic Committee, Heilongjiang Medical Association; the Director of the Chinese Plastic and Cosmetic Association; the Executive Director of the Oral Plastic and Cosmetic Branch, Chinese Plastic and Cosmetic Association; and the Director of the Academic Committee of the Sino-Russian Medical University Union. He is also a member of the Organizing Committee of the National Conference on Aesthetic Oral Medicine and the 9th Annual Aesthetic Dentistry Academic Conference. He also serves as an Expert Reviewer for the national core journal *China Tissue Engineering Research*. He has spoken at the Orthodontic Conference many times.